FEATURE ARTICLE

Bandwidth extension of seismic data and its impact on seismic attribute computation

Satinder Chopra, Ritesh Kumar Sharma*, John P. Castagna+ and Kurt J. Marfurt†*

Abstract

Bandwidth extension of seismic data is a desirable goal when the available data has inadequate frequency content. Though significant efforts are expended during processing of seismic data to preserve the frequency content, they may not be effective enough to resolve reservoir intervals below tuning. We describe the performance of the *sparse layer seismic reflectivity inversion* to extend the seismic bandwidth. This method yields a reflectivity series, which can be subsequently filtered to a desirable bandwidth that provides optimum resolution. These broader band results give reasonably accurate synthetic ties to wells and can also be used to derive relative acoustic impedance. By tightening the seismic wavelet and enhancing lateral changes in phase, bandwidth extension also improves lateral resolution as measured by volumetric dip, coherence, and curvature attributes. Given these improvements, we apply two different unsupervised machine learning methods to attributes computed from the bandwidth extended data and compare them to the results computed from the original data. We find bandwidth extension provides a higher level of detail, whether it is the lineaments corresponding to faults or the thin-layered lithointervals than classification of the original data.

Keywords: bandwidth extension, seismic attributes, machine learning, self-organizing mapping, generative topographic mapping

Introduction

During the last decade, the developments in broadband acquisition and processing for land and marine seismic data have demonstrated the importance of enhanced signal bandwidth. The processing of such broadband data comes with its challenges, a salient one being noise attenuation at low frequencies for gaining signal bandwidth. Bandwidth extension processing when carried out post-imaging, can facilitate seismic interpretation, attribute analysis and reservoir characterization, and can benefit both legacy and modern broadband seismic data.

In this paper we describe the sparse layer seismic reflectivity inversion method (Zhang and Castagna, 2011) for bandwidth extension. This method makes use of the basis pursuit decomposition and is superior to the traditional way of broadening the seismic bandwidth with application of spiking deconvolution. The inversion method determines a sparse number of reflectivity patterns, which when summed together form the original seismic trace. The determined pattern on convolution with a wavelet of extended bandwidth yields the desired bandwidth extension. The details of the method are discussed in the next section.

Next, we demonstrate the advantages that accrue by performing bandwidth extension on a 3D seismic dataset (along with data for two wells falling on the 3D survey) from Smeaheia area in offshore Norway. The first advantage is in terms of reasonably accurate synthetic ties to wells, followed by the second advantage in that

*SamiGeo Consulting Ltd., Calgary, Alberta. Email: Satinder.Chopra@samigeo.com
*SamiGeo Consulting Ltd., Calgary, Alberta. Email: Ritesh.Sharma@samigeo.com
*University of Houston, Texas. Email: jcastagnaou@yahoo.com
*University of Oklahoma, Oklahoma. Email: kmarfurt@ou.edu

the seismic attributes generated on the bandwidth extended data exhibits improved lateral resolution. We demonstrate this with the generation of attributes such as relative acoustic impedance, multispectral energy ratio coherence, and multispectral curvature.

Finally, we take the exercise forward by generating a number of attributes (relative acoustic impedance, instantaneous amplitude, instantaneous frequency, GLCM energy and spectral magnitude at different frequencies) on both the input as well as the bandwidth extended versions of the seismic data. The generated attributes are then used to perform unsupervised machine learning facies classification using three of the known methods such as k_{means}, *self-organizing mapping* (SOM) and *generative topographic mapping* (GTM). On comparing the stratal displays extracted from the facies volumes so generated, we find that the facies generated on bandwidth extended data yield higher spatial resolution, whether it is the lineaments corresponding to faults or the thin-layered lithointervals.

In view of such observations, it would not be incorrect to say that bandwidth extension is an enabler for application to narrow band legacy seismic data. Modern broadband seismic data have a wider band of frequencies than the legacy seismic data but may still fall short of expectation for thin reservoir targets. In those cases, bandwidth extension could prove to be useful as well.

Sparse layer seismic reflectivity inversion

In the *sparse-layer seismic reflectivity inversion method* (Zhang and Castagna, 2011) a temporally and spatially varying wavelet estimate is made. Just as an isolated spike (with an unknown wavelet) forms the basis function in spiking deconvolution, a library of thin-bed responses comprising dipole (2 layer or thin bed) basis functions (layer responses) are convolved with the wavelet field using *a priori* information and statistical assumptions. The basis functions are then fit to the data using a least-squares fit criterion. The sparse layer inversion determines a sparse number of patterns which when summed together form the original seismic trace. To extend the bandwidth, we now use the same dipoles that were convolved with the original wavelet field, but now replace the original wavelet with one with an extended bandwidth. Explicitly stated, the algorithm replaces the original data with a model of dipoles convolved with the well-log generated synthetic wavelet or statistical wavelet with a wavelet of our own choosing. In this manner, the unmeasured high and low frequencies in the new extended bandwidth wavelet are consistent with the same model used to represent the original data.

The sparse layer inversion does not directly use well data in the inversion, though well data may be used in wavelet extraction and parameter selection (such as degree of sparsity), and of course for validation. By operating on a trace-by-trace basis, this inversion yields a reflectivity series, which is then filtered to a desirable bandwidth that exhibits an optimum combination of resolution and reasonably accurate synthetic ties to wells. The output reflectivity series can also be used to derive relative acoustic impedance.

We use the 3D seismic data from Smeaheia area in offshore Norway to demonstrate the value of sparse layer inversion, where the Smeaheia area is a candidate for CO_2 storage and evaluation.

The Smeahiea area lies about 30 km east of the Troll gas field (Figure 1), within the Norwegian continental shelf. It is located in a fault block bounded by the Vette Fault to the west and the Øygarden Fault to the east and is raised about 300 m relative to the Troll field. The Late Jurassic Sognefjord, Fensfjord, and Krossfjord formations form the producing reservoir zones in the Troll gas field.

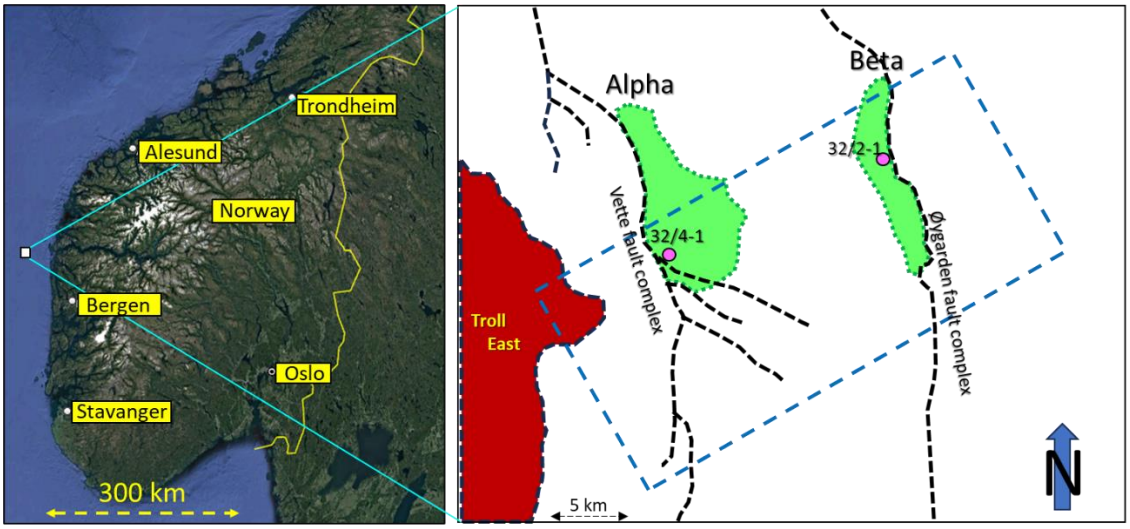

Figure 1: (Left) Location of the Smeaheia area on the Norwegian continental shelf. (Right) Zoom of the Smeaheia area indicating the two interpreted structures, 'Alpha' and 'Beta'. The two main fault complexes in the area are marked as dashed black lines. The dashed blue rectangle depicts the outline of the 3D seismic volume being used. The image to the left was prepared with the use of Google Earth Pro. (Modified after Furre et al., 2017)

In the Smeaheia block, there are two four-way closure structures, the Alpha structure to the west and the Beta structure to the east. Two exploration wells, namely 32/4-1 and 32/2-1 have been drilled into these structures, and although the reservoir is good, both wells turned out to be dry, indicating that the Smeaheia area is not charged with hydrocarbons.

In the Smeaheia area, the Sognefjord Formation is the primary reservoir consisting of medium to coarse-grain, well-sorted, micaceous, and minor argillaceous sandstone. Below this formation lies the Fensfjord Formation consisting of medium-grained, well-sorted sandstone with shale intercalations. Underlying the Fensfjord Formation is the Krossfjord Formation with medium to coarse-grained, well-sorted sandstone.

Overlying the Sognefjord Formation are the Heather and Draupne formation shales. While the Heather formation comprised of silty claystone with thin streaks of limestone interfingering the Sognefjord, Fensfjord and Krossfjord sandstones. The Draupne Formation consists of dark grey to brown/black shale that is non-calcareous, carbonaceous, and fissile claystone. Both the Heather and Draupne formations serve as primary seals for the proposed CO_2 storage reservoir sandstones of the Sognefjord, Fensfjord and Krossfjord formations.

As the Sognefjord, Fensfjord and Krossfjord are sandstone reservoir formations, there is concern about evaluation of their properties for thicknesses that fall below seismic resolution, which could come from shale and carbonate stringers within these zones. Finally, the existence of faults/fractures that fall below seismic resolution could provide pathways for fluid losses. All these risks need to be evaluated and mitigated in the context of long-term CO_2 storage.

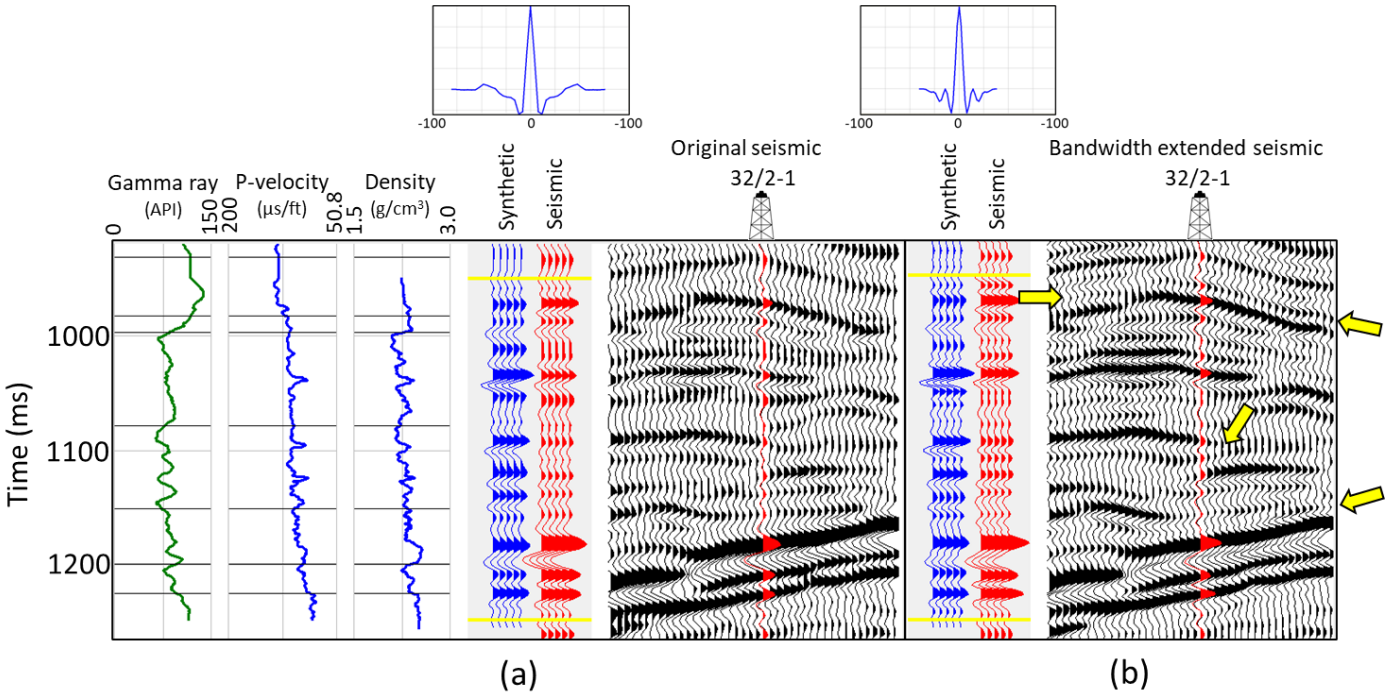

Figure 2: Correlation of well curves with seismic data. The blue traces represent the synthetics (generated with the wavelet shown above), whereas the red traces represent the seismic data (a) before, and (b) after bandwidth extension. The correlation coefficients for the ties were 0.745 for (a) and 0.756 for (b). Thus, there is a good correlation between the synthetic and red traces in the time window indicated for both data volumes but note the resolution of additional events after bandwidth extension indicated by the yellow arrows.

Available data for demonstration of bandwidth extension

The available seismic data were the GN1101 3D survey covering the Smeaheia (blue dashed rectangle shown in Figure 1) acquired by Gassnova in 2011 made publicly available by Gassnova and Equinor. The bin size for the data is 12.5 x 25 m, with a sample interval of 4 ms. Gassnova provided interpreted horizons and well log data for the two 32/4-1 and 32/2-1 wells along with well completion reports. These logs consisted of the complete gamma ray curves, but the sonic and density logs were not recorded for the shallower depths. The seismic data volume is of good quality.

Figure 2 shows the correlation of well curves with seismic data. The blue traces represent the synthetic seismograms generated with the zero-phase wavelet shown above. The red traces represent the seismic data (a) before, and (b) after bandwidth extension. Windows of seismic data before and after bandwidth extension from where the red traces are extracted are also shown alongside. There is a reasonably good correlation between the synthetic and red traces in the time window for the bandwidth extended data; furthermore, there are more reflection cycles.

Figure 3a shows a segment of an inline seismic section extracted from the available seismic data volume (which has a bandpass filter applied), which passes through well 32/4-1 and exhibits the different markers overlaid. The gamma ray curve for well 32/4-1 is shown overlaid on the section.

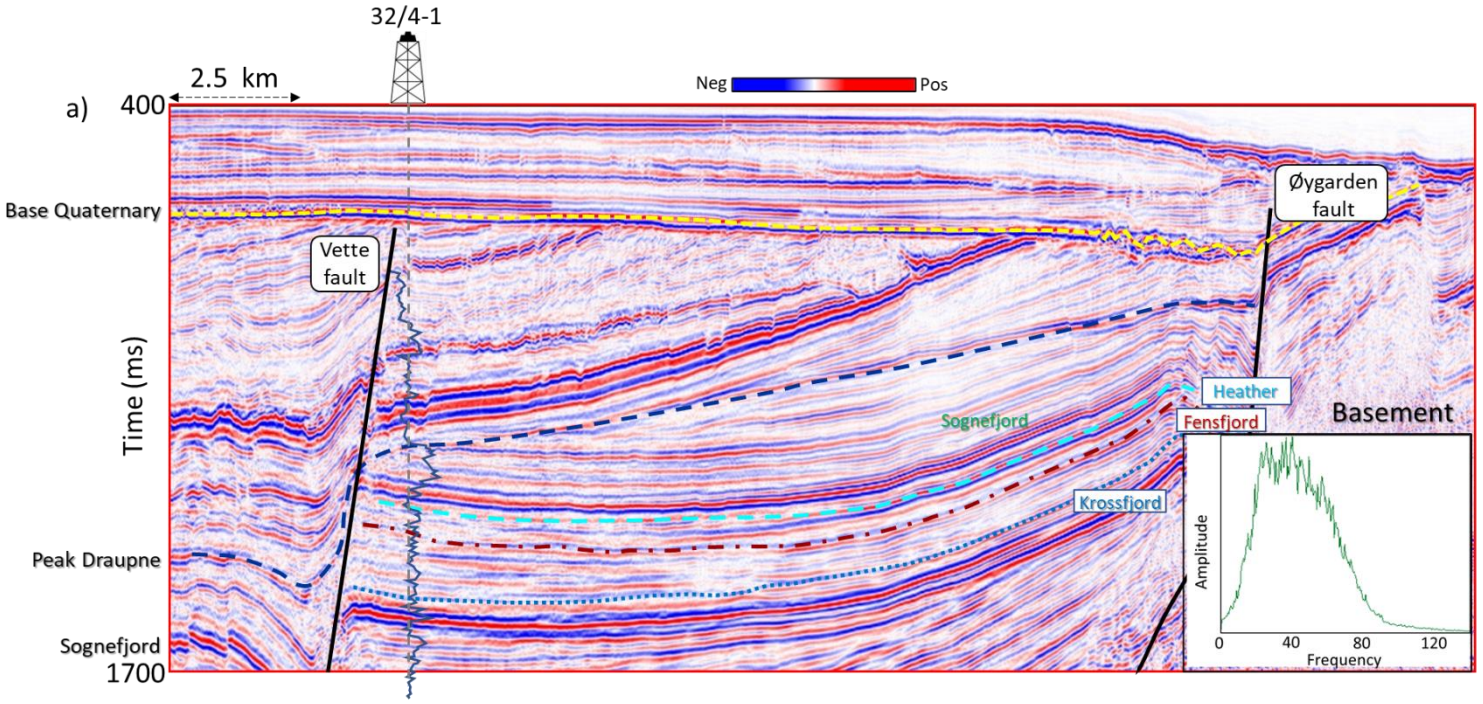

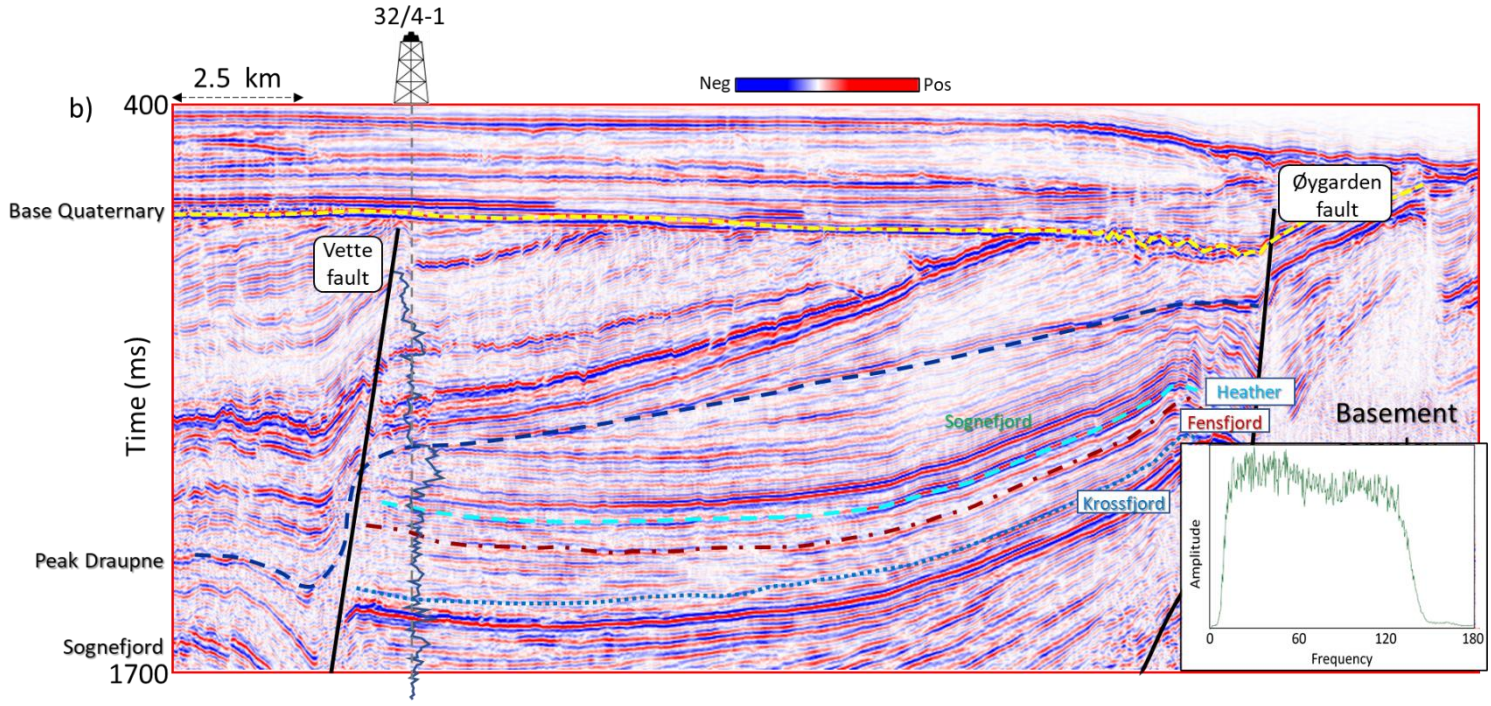

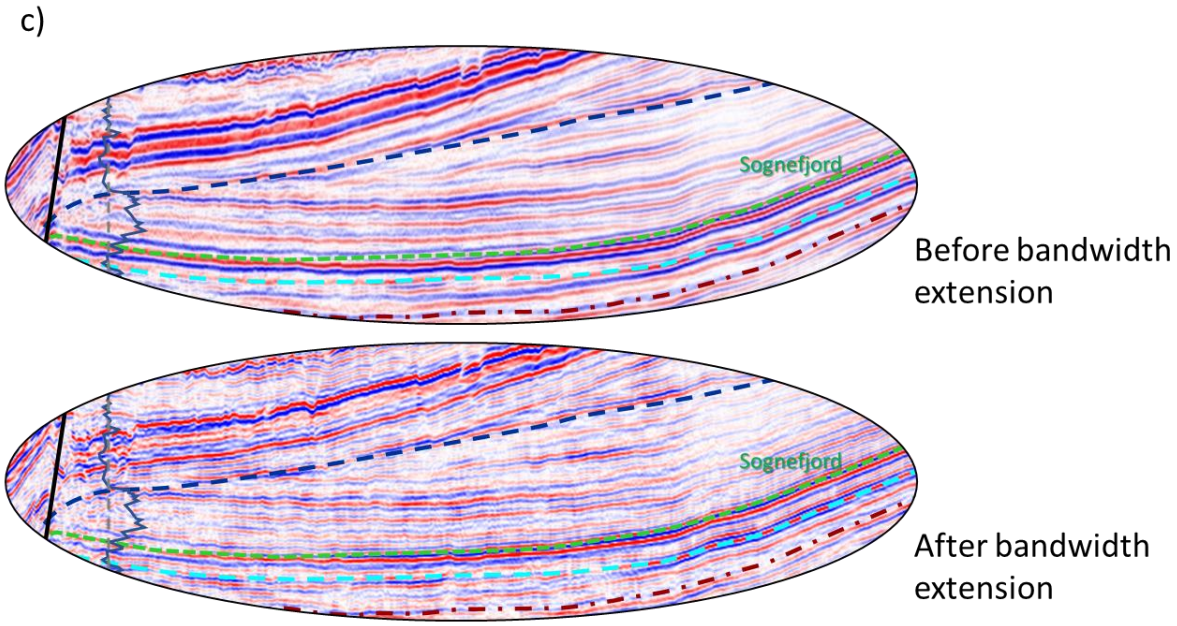

Figure 3: Segment of an inline extracted from (a) input seismic data volume, and (b) input seismic data volume after bandwidth extension. Some relevant markers and gamma ray curve for well 32/4-1 are overlaid on the two sections. (c) Zoom of the two sections cropped to the area enclosed by the black oblong shapes on the two images clearly shows the higher frequency content after bandwidth extension. The frequency spectra (computed over the time window exhibited and over the whole seismic volume) for the two data volumes are also shown to the right. Notice the enhancement in the resolution of the reflections after bandwidth extension. Notice, the low and higher frequencies after bandwidth extension contribute to the higher resolution.

The 'Base Quaternary' (in yellow) represents an angular unconformity, and the 'Peak Draupne' (in dark blue) the top of the shale formation. The 'Sognefjord' (in green), 'Fensfjord (in cyan) and 'Krossfjord' (in bluish green) are the markers of interest representing sandstone formations as described above. Two prominent faults in solid black (Vette fault to the west and Øygarden fault to the east) are also shown overlaid on the section. The frequency spectrum computed for the time interval of the seismic data exhibited is shown to the right, which indicates a roll-off of the frequencies beyond 40 Hz. The bandwidth extension method employed here uses the spectrum ranging from 5-80 Hz to define a model (the weights in the fit are the spectral magnitudes in Figure 3a, so the 40 Hz is weighted more than 80 Hz). After 80 Hz the model *extends* the spectrum from 80 to 140 Hz where no data were measured.

Generation of different attributes

With the improved vertical resolution seen in Figure 3b, our next task is to determine if bandwidth extension also enhances the lateral resolution as measured by seismic attributes such as coherence and curvature. Specifically, we anticipate that some lateral discontinuities fall near the limits of seismic resolution in the original data but will be better resolved in the bandwidth extension data.

Energy ratio coherence: Encouraged with the higher-frequency content of the seismic data, we first generated the coherence attribute. Much has been written about this attribute and the usefulness of its application. We make use of the multispectral energy ratio-based coherence algorithm for which more details can be found in Chopra and Marfurt (2008; 2018a, 2018b, 2019) and Li and Lu (2018).

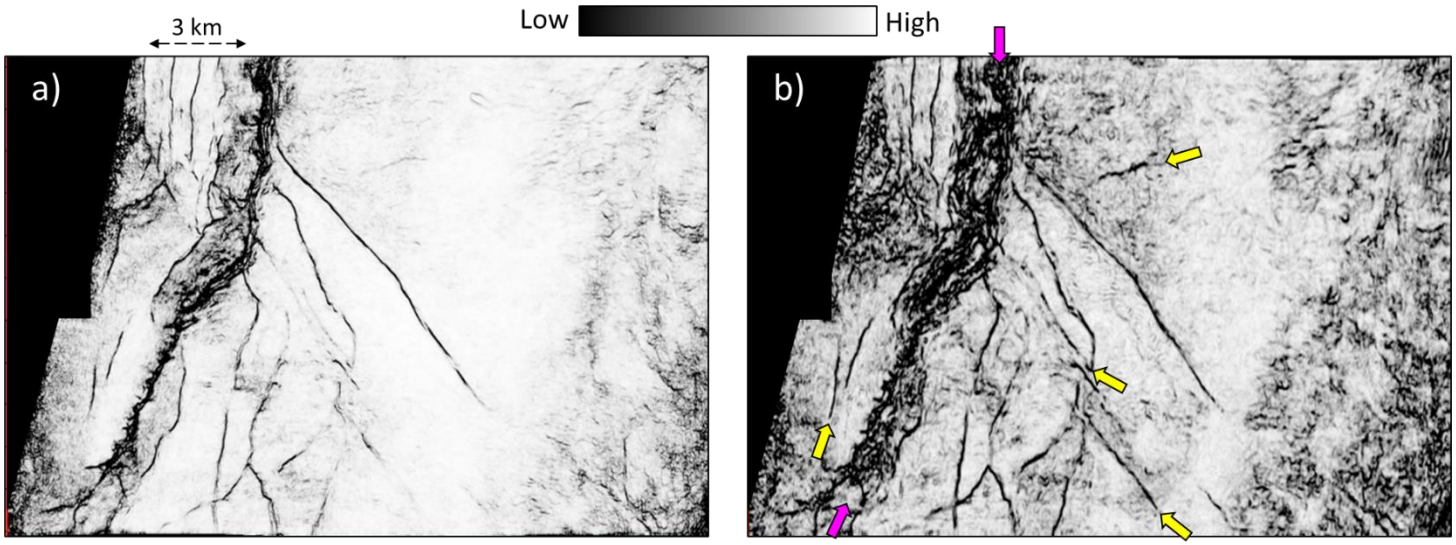

Figure 4: Time slice at 1.66 s through multispectral energy ratio coherence volumes computed on (a) input seismic data with structure-oriented filtering, and (b) input seismic data with bandwidth extension and structure-oriented filtering. Notice the superior definition of the lineaments in terms of their continuity and intensity seen on the display in (b). Some of the weak lineaments seen in (a) are better delineated in (b) indicated by yellow arrows. The fault damage zone indicated by magenta arrows is better defined in (b).

Similarly, we generated the multispectral curvature attribute (more details can be found in the Al-Dossary and Marfurt ,2006; Chopra and Marfurt, 2007; 2010) and noticed superior definition of the lineaments in terms of their continuity, intensity and resolution seen on the displays (not shown here).

Relative acoustic impedance is computed by continuous integration of the original seismic trace with the subsequent application of a low-cut filter. Because it assumes a zero-phase wavelet that is as close to a spike as possible, the improved resolution of bandwidth extension will provide improved results over the original data. The impedance transformation of seismic amplitudes enables the transition from reflection interface to interval properties of the data, without the requirement of a low-frequency model. A comparison of stratal slices 32 ms above the Sognefjord marker from the relative acoustic impedance attributes computed from input seismic data and input seismic data after bandwidth extension is shown in Figure 5. Notice the crisp definition of the faults as indicated by the highlighted areas in dashed purple outlines.

Likewise, the other attributes computed on the two seismic volumes are listed below along with their brief descriptions.

Instantaneous envelope/frequency: Instantaneous envelope is a measure of the instantaneous energy of the analytic seismic trace, independent of phase, and provides information on intensity of reflections. Similarly,

instantaneous frequency provides information on attenuation and layer thickness. We use a smoother, more stable version of the instantaneous frequency usually obtained by weighting it by the envelope.

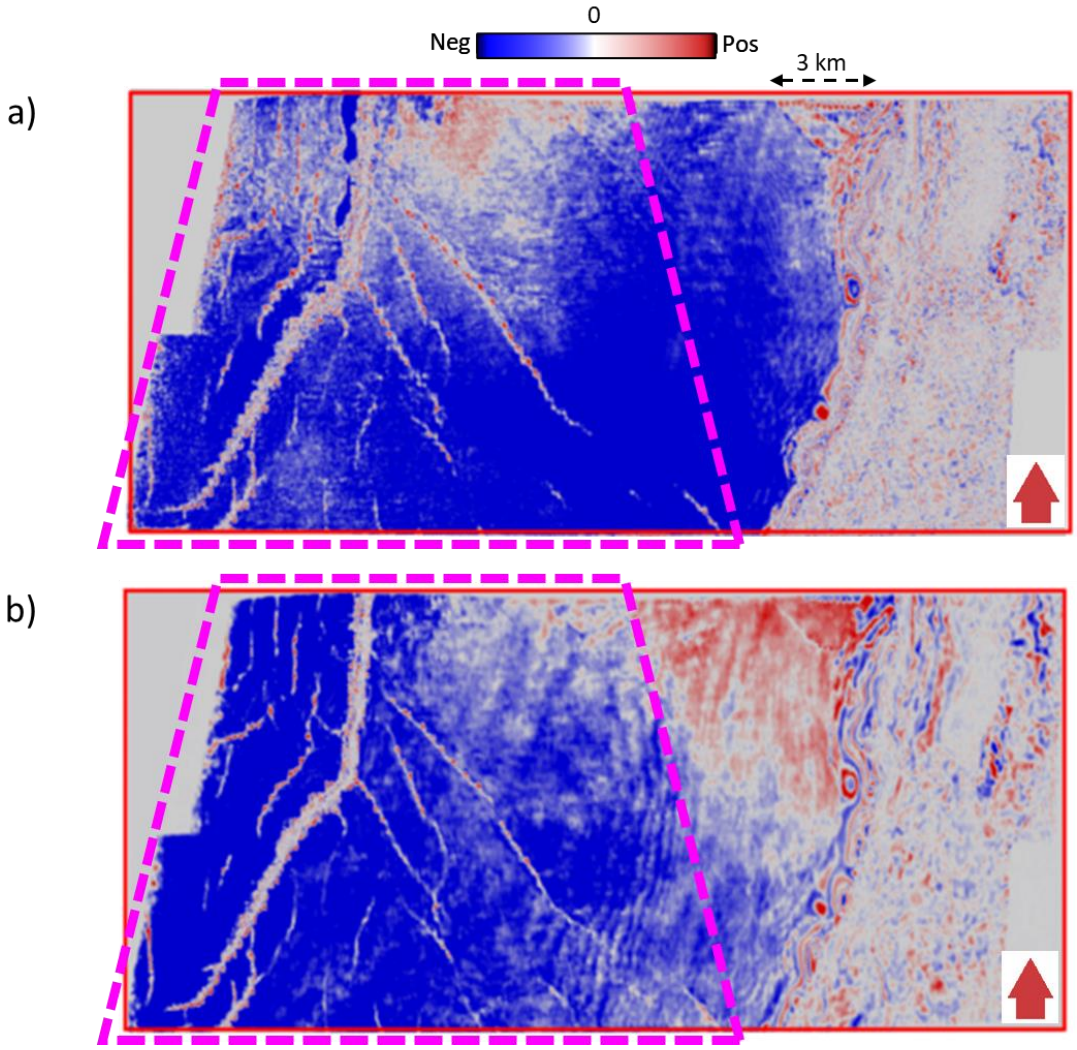

Figure 5: Stratal slice 32 ms above the Sognefjord marker from the relative acoustic impedance attributes computed from (a) input seismic data, and (b) input seismic data after bandwidth extension. Notice the crisp definition of the faults highlighted areas in dashed purple outline in (b).

Sweetness: Sweetness is a "meta-attribute" or one computed from others, which in this case is the ratio of the envelope to the square root of the instantaneous frequency. A clean sand embedded in a shale will exhibit high envelope and lower instantaneous frequency, and thus higher sweetness, than the surrounding shale-on-shale reflections.

GLCM Energy: GLCM or grey-level co-occurrence matrix energy is a measure of textural uniformity in the data. If the reflectivity along a horizon is nearly constant, it will exhibit high GLCM energy.

Spectral magnitude: The magnitude of spectral components ranging from 20 Hz to 70 Hz, which is the effective bandwidth of the input seismic data.

Specifically, the attributes used for the computation of seismic facies classification using some of the unsupervised machine learning methods were the relative acoustic impedance, envelope, sweetness, GLCM energy and spectral magnitudes at 25 Hz, 40 Hz and 55 Hz.

All these different attributes have been generated on both the input seismic and the bandwidth extended versions to use them as input for unsupervised seismic facies classification using machine learning techniques, which are described in the next section.

Seismic facies classification using machine learning techniques on input seismic, and bandwidth extended seismic data

We apply two different unsupervised seismic facies classification machine learning methods, namely *self-organizing mapping* (SOM), and *generative topographic mapping* (GTM), to them. A comparison of the two versions reveals supervisor spatial facies resolution as well as crisp definition of faults/fractures as seen on the bandwidth extended seismic data.

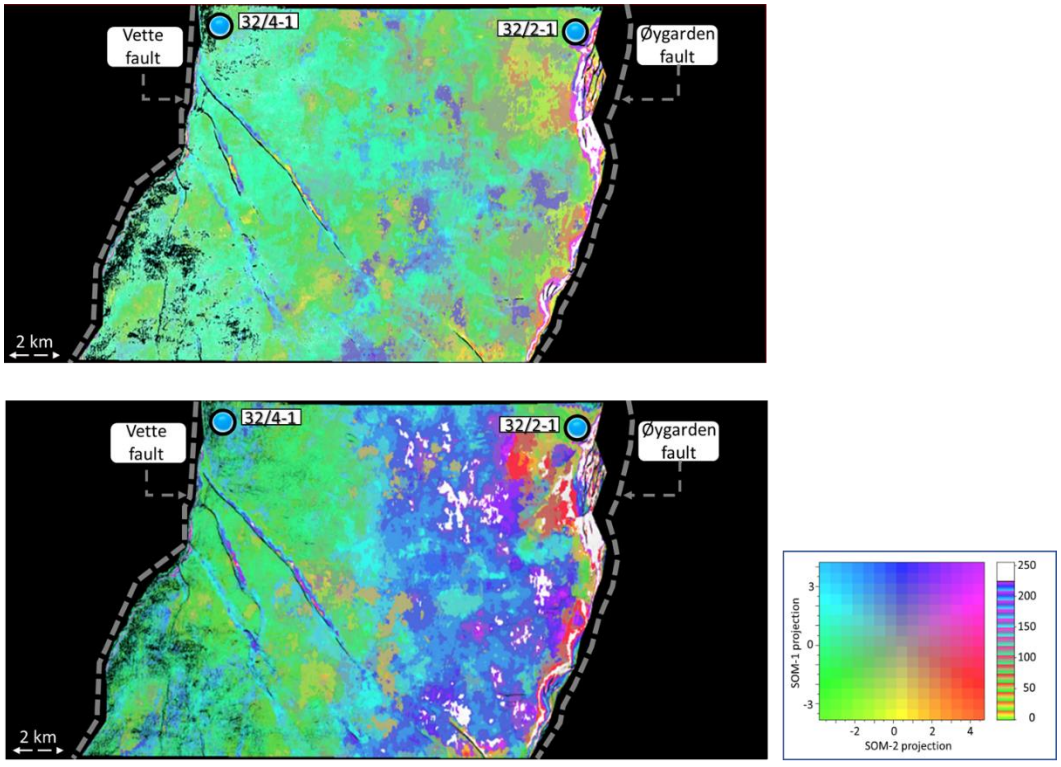

Figure 6: Stratal slice at 228 ms below the Sognefjord marker (within Krossfjord Fm) extracted from the SOM crossplot volume computed on attributes generated on (a) input seismic data volume, and (b) bandwidth extended input seismic data volume. The two displays have been corendered with the respective multispectral energy ratio coherence attribute volumes. Better spatial resolution of the seismic facies is seen in (b) than in (a). Only the target area between the Vette and Øygarden faults was classified and has been shown.

The brief description of both these methods is given below, but more details can be found in Chopra et al. (2022).

Self-organizing mapping

SOM is an unsupervised machine learning technique based on the clustering approach that generates a seismic facies map from multiple seismic attributes. In this technique the initial cluster centroids are defined in an N-dimensional attribute data space by fitting a plane defined by the first two eigen vectors of the covariance matrix (Kohonen, 1982, 2001) to the data in a least-squares sense. With centroid still locked to this plane, it is iteratively deformed into a 2-D surface that fits the data still better. Once convergence is reached, the N-dimensional data are projected onto this 2-D surface. Thus, SOM may be considered as projection from a multidimensional attribute space to a 2-D space or "latent" (hidden) space. Usually, the output from SOM computation is obtained in the form of two projections on the two SOM axes, which can then be directly crossplotted and displayed using a 2-D RGB color bar.

Figure 6 shows the equivalent stratal displays (within the Krossfjord formation) extracted from the SOM crossplot volume computed for the input and bandwidth extended versions of the seismic data, using a 2D color bar. Some of the clusters seen on the display in Figure 6b are better defined than the ones shown in Figure 6a. Thus, a superior distribution of the seismic facies corresponding to the different colours for the SOM seismic facies generated on the bandwidth extended version is seen.

Generative topographic mapping

Though the Kohonen SOM method described above is easy to implement, is computationally inexpensive, and thus is a popular unsupervised clustering approach, it does have limitations. First, there is no theoretical basis for the selection of parameters such as training radius, neighborhood function and learning radius, as all of these are data dependent (Bishop et al., 1998; Roy, 2013). Secondly, no cost function is defined in the method that could be iteratively minimized indicating convergence during the training process.

Finally, as a measure of confidence in the final clustering results, no probability density is defined. An alternative approach to the Kohonen SOM method, called "generative topographic mapping," overcomes the above-stated limitations (Bishop et al., 1998). It is a nonlinear dimension reduction technique that provides a probabilistic representation of the data vectors in latent space.

In Figure 7 we show the displays equivalent to those shown for SOM analysis, where some of the clusters can be interpreted with ease with less background clutter and confusion.

In the comparison of the seismic facies displays generated for the original seismic data as well as the bandwidth extended version and shown above at different levels we see almost no variation of facies carried out on the former, but a definite variation of seismic facies carried out on the latter from well 32/4-1 to the left to well 32/2-1 to the right. To ascertain such a variation, we picked up the available well data at the two wells and carried out Bayesian facies classification. Figure 18a shows a crossplot of porosity against gamma-ray well curves. The data points in blue come from well 32/4-1 and the yellow ones from well 32/2-1. Based on the cutoff values for porosity and gamma-ray, five coloured ellipses enclose clusters of points assigned based on Bayesian classification. When backprojected on the curves for the two wells they highlight zones based on the colour of the cluster they represent. We notice that the red facies in well 32/4-1 is seen more as green in the same zone in well 32/2-1 in the Sognefjord, Heather, Fensfjord and Krossfjord intervals, which suggests

different facies in the two wells at these levels. This lends support to the facies variation we see after bandwidth extension of seismic data.

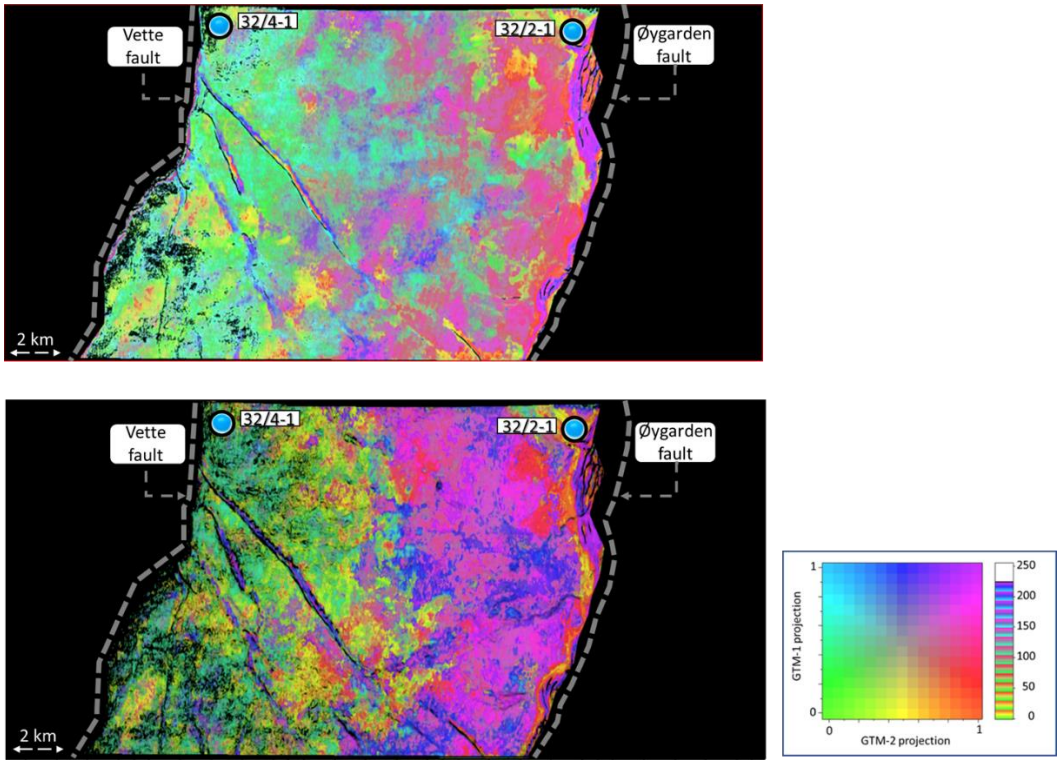

Figure 7: Stratal slice at 228 ms below the Sognefjord marker (within Krossfjord Fm) extracted from the GTM crossplot volume computed on attributes generated on (a) input seismic data volume, and (b) bandwidth extended input seismic data volume. The two displays have been corendered with the respective multispectral energy ratio coherence attribute volumes. Better spatial resolution of the seismic facies is seen in (b) than in (a). Only the target area between the Vette and Øygarden faults was classified and has been shown.

Conclusions

We have found that bandwidth extension of the input seismic data improves not only the vertical resolution seen on vertical amplitude slices but also the lateral resolution of subsequent attributes computations displayed as time and horizon slices. Results obtained for the unsupervised machine learning applications employing both the input seismic as well as its bandwidth extended version depict superior performance of the latter in terms of clarity of clusters as well as color variations within them. Such an observation seems to agree with the observation about variation in facies from the well to the west of the seismic volume to the well to the east.

Applications of SOM and GTM techniques to the same data allowed us to assess their relative strengths as well as their suitability. We found that both GTM has an edge over SOM in terms of the detailed distribution of seismic facies in terms of better resolution and distinct definition of the geologic features seen on the displays.

Usually, the seismic facies maps in the zones of interest are calibrated with the lithofacies information obtained from well cores and cuttings. As there is appreciable difference in resolution between the two types of data, it is advisable to enhance the resolution of seismic data by adopting a bandwidth extension workflow. Such a

workflow can narrow down the resolution gap between the facies data types (seismic and geologic) as well as help perform a better correlation/calibration between the two.

Though the analysis is qualitative at present, it paves the way for more detailed work as more well and production data become available.

Acknowledgements

The bandwidth extension work discussed in this paper employed the Ultra™ module owned by Lumina Technologies, Houston. The first author would also like to thank the Attribute-Assisted Seismic Processing and Interpretation (AASPI) Consortium, University of Oklahoma, for access to their software, which has been used for all attribute computation as well as subsurface AI (formerly Geomodeling Technology Corp.), Calgary, for making the Attribute-Studio™ software available. We wish to thank Gassnova and Equinor for access to the Smeaheia 3D seismic and other associated data used in this exercise.

References

Al-Dossary, S. and K. J. Marfurt, 2006, 3-D volumetric multispectral estimates of reflector curvature and rotation. Geophysics, **71**(5), 41–51. https://dx.doi.org/10.1190/1.2242449.

Bishop, C. M., M. Svensen, and C. K. I. Williams, 1998, The generative topographic mapping: Neural Computation, **10**(1), 215-234.

Chopra, S., and K. J. Marfurt, 2007, Seismic Attributes for Prospect Identification and Reservoir Characterization, SEG.

Chopra, S. and K. J. Marfurt, 2010, Integration of coherence and volumetric curvature images. The Leading Edge, **29**(9), 1092-1107, https://dx.doi.org/10.1190/1.3485770

Chopra, S., and K. J. Marfurt, 2008, Gleaning meaningful information from seismic attributes: *First Break*, **26**(9), 43–53, http://dx.doi.org/10.3997/1365-2397.2008012

Chopra, S., and K. J. Marfurt, 2019, Multispectral, multiazimuth, and multioffset coherence attribute applications: *Interpretation*, **7**(2), SC21-SC32. http://dx.doi.org/10.1190/INT-2018-0090.1.

Chopra, S., and K. J. Marfurt, 2018a, Coherence attribute applications on seismic data in various guises — Part 1: *Interpretation*, **6**(3), T521-T529. http://dx.doi.org/10.1190/INT-2018-0006.1.

Chopra, S., and K. J. Marfurt, 2018b, Coherence attribute applications on seismic data in various guises — Part 2: *Interpretation*, **6**(3), T531-T541. http://dx.doi.org/10.1190/INT-2018-0007.1.

Chopra, S., R. K. Sharma, K. J. Marfurt, H. Bedle, and S. Verma, 2022, Attempts at seismic characterization of a deepwater turbidite channel in Taranaki Basin, New Zealand, First Break, 40(10), 27-39. https://doi.org/10.3997/1365-2397.fb2022080.

Furre, A., S. Bussat, P. Ringrose, and R. Thorsen, 2017, Optimizing monitoring strategies for contrasting offshore CO2 storage sites, in EAGE/SEG workshop on CO_2 storage monitoring.

Kohonen, T., 1982, Self-organized formation of topologically correct feature maps: *Biological Cybernetics,* **43**, 59-69.

Kohonen, T., 2001, *Self-organizing Maps*: Springer-Verlag.

Li, F. Y., and W. K. Lu, 2014, Coherence attribute at different spectral scales: *Interpretation*, **2**(1), SA99–SA10. http://dx.doi.org/10.1190/INT-2013-0089.1.

Roy, A., 2013, Latent space classification of seismic facies: Ph.D. Dissertation, The University of Oklahoma.

Roy, A., A. S. Romero-Peleaz, T. J. Kwiatkowski, and K. J. Marfurt, 2014, Generative topographic mapping for seismic facies estimation of a carbonate wash, Veracruz Basin, southern Mexico, Interpretation, 2(1), SA31-SA47. http://dx.doi.org/10.1190/INT-2013-0077.1.

Zhang, R., and J. P. Castagna, 2011, Seismic sparse-layer reflectivity inversion using basis pursuit decomposition. Geophysics, **76**(6), R147-R158. http://doi:10.1190/GEO2011-0103.1

Satinder Chopra: His photo and bio are available on page 79.

Ritesh Kumar Sharma received his master's and Ph.D. degrees in geophysics from the University of Calgary. He has worked as senior reservoir geoscientist at TGS, Canada till 2020, and now works for SamiGeo Consulting Ltd. at Calgary. Ritesh has vast experience in working with applications such as AVO analysis (including azimuthal AVO), rock-physics analysis, frequency enhancement of seismic data, simultaneous inversion, extended elastic impedance inversion as well as geostatistical inversion. He has delivered many oral and poster presentations and published several papers in renowned journals. He has won the **best poster award** for his presentation at the 2012 GeoConvention held at Calgary, the **Jules Braunstein Memorial Award** for the best AAPG poster presentation at the 2013 AAPG Convention held at Pittsburgh, **CSEG Honorable Mention** for **the Best Recorder Paper award** in 2013 and is the recipient of **Honorable Mention Best Poster Paper** in SEG 2017. He is an active member of SEG and CSEG.

John P. Castagna specializes in exploration geophysics research and development. He is widely known for his work in direct hydrocarbon detection and reservoir characterization. John is a graduate of Brooklyn College, where he earned a B.S. in geology in 1976 and an M.S. in high-temperature geochemistry in 1981. He completed his doctoral degree in exploration geophysics at the University of Texas at Austin in 1983. During his career, he has held several positions at ARCO research and Vastar resources. In 2000 and 2010, he founded Fusion Geophysical and Lumina Geophysical, respectively. He was named a distinguished lecturer for SEG, delivering the fall lecture on "Applied AVO analysis: use and abuse of amplitude variation with offset." He has served SEG in various other capacities including chairman of *The Leading Edge* editorial board, first vice-president, and technical program chairman for the 2003 Annual Convention in Dallas, and associate editor for GEOPHYSICS. He has written two book, *Offset-dependent-reflectivity: Theory and practice of AVO analysis*, and *AVO*. He currently holds the Robert Sheriff Chair of Geophysics at the University of Houston.

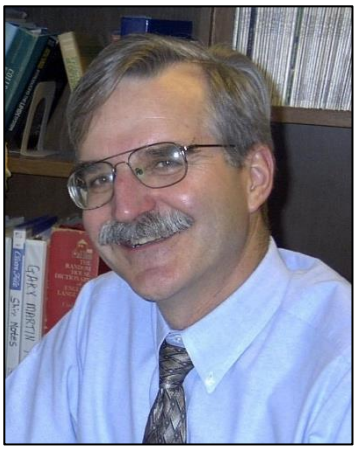

Kurt J. Marfurt received a Ph.D. (1978) in applied geophysics from Columbia University's Henry Krumb School of Mines in New York, where he also taught as an assistant professor for four years. He joined the University of Oklahoma (OU) in 2007, where he served as the Frank and Henrietta Schultz professor of geophysics within the ConocoPhillips School of Geology and Geophysics and is now Emeritus Professor there. He worked for 18 years in a wide range of research projects at Amoco's Tulsa Research Center, after which he joined the University of Houston for eight years as a professor of geophysics and the director of the Allied Geophysics Lab. He has received the following recognitions: SEG best paper (for coherence), SEG best presentation (for seismic modeling), as a coauthor with Satinder Chopra for best SEG poster (for curvature) and best AAPG technical presentation, and as a coauthor with Roderick Perez-Altamar for best paper in *Interpretation* (on a resource play case study). He also served as the SEG/EAGE Distinguished Short Course Instructor for 2006 and 2018.

Glacial moraine in Shyok Valley, Ladakh, India. A moraine is a material left behind by a moving glacier. This material is usually soil and rock. Just as rivers carry along all sorts of debris and silt that eventually builds up to form deltas, glaciers transport all sorts of dirt and boulders that build up to form moraines. (Photo courtesy: Ritesh M. Joshi)